ARTICLE OPEN

Off-resonant detection of domain wall oscillations using deterministically placed nanodiamonds

Jeffrey Rable[1], Jyotirmay Dwivedi[1] and Nitin Samarth[1,2,3 ✉]

Nitrogen-vacancy (NV) centers in diamond offer a sensitive method of measuring the spatially localized dynamics of magnetization and associated spin textures in ferromagnetic materials. We use NV centers in a deterministically positioned nanodiamond to demonstrate off-resonant detection of microwave field-driven GHz-scale oscillations of a single domain wall (DW). The technique exploits the enhanced relaxation of NV center spins due to the broadband stray field noise generated by an oscillating DW pinned at an engineered defect in a lithographically patterned ferromagnetic nanowire. Discrepancies between the observed DW oscillation frequency and predictions from micromagnetic simulations suggest extreme sensitivity of DW dynamics to patterning imperfections such as edge roughness. These experiments and simulations identify potential pathways toward quantum spintronic devices that exploit current-driven DWs as nanoscale microwave generators for qubit control, greatly increasing the driving field at an NV center and thus drastically reducing the π pulse time.

INTRODUCTION

GHz-scale ferromagnetic dynamics, such as spin waves, vortex gyrations, and domain wall oscillations, offer both a fascinating target for quantum sensing and a potential qubit-driving source in quantum computing applications. One of these qubits, the nitrogen-vacancy (NV) center in diamond, has been previously used to detect ferromagnetic resonance[1–4], spin-wave scattering[5], spin-wave frequency multiplication[6], and vortex gyrations[7]. Ferromagnetic dynamics have also been explored as potential sources of microwave driving for NV centers: NV-magnon coupling was first reported in 2017[8], then electrically tuned in subsequent works[9,10], and vortices have been shown to enhance NV spin rotation during qubit addressability experiments[11].

Domain walls (DWs) should offer similar advantages to vortices for addressability since they produce large stray fields and can be moved electrically. Pinned DWs act like a mass in a potential well, which is determined by the ferromagnet's properties; they can oscillate in the GHz range, making them useful for direct NV driving. They can be pinned to specific sites via geometric patterning of the magnetic feature and can be driven via external microwave fields[12], DC current[13,14], AC current[15], and spin transfer torques[16]. However, the literature on DW sensing using NVs has been largely focused on characterizing their static structures[17–19].

The goal of this paper is to establish a platform and methodology that will ultimately allow the resonant measurement and manipulation of a single trapped oscillating DW. This could form the basis for quantum technology components such as a nanoscale microwave amplifier or generator. To this end, we demonstrate an important first step, namely the off-resonant detection of GHz-scale oscillations of a single transverse DW pinned at a defect in a ferromagnetic nanowire. The detection is carried out using spin relaxometry measurements (pulsed optically detected magnetic resonance) of NV centers located in a nanodiamond that is deterministically positioned near the DW (Fig. 1) via a pick-and-place protocol reported recently[4]. Our platform uses NiFe (Permalloy, Py) patterned into a semicircular

nanowire with a centrally positioned notch; this allows us to probe a pinned single DW which is nucleated at the notch by applying a radially directed external magnetic field. The geometry inherently allows control measurements by using a tangential external magnetic field to destroy the DW. We demonstrate that, like previous ferromagnetic resonance and vortex gyration measurements[7], driving of DW oscillations generates magnetic fields that overlap the NV ground state transition frequency, reducing NV polarized state lifetimes and producing an optical contrast.

RESULTS

We first used micromagnetics simulations to model the DW dynamics in semicircular Py nanowires with a defect (see Methods). This guided the experimental design of an optimal nanowire/notch geometry wherein the DW dynamics are in an ideal range for NV center-based detection and will also eventually allow for maximum resonant coupling. These simulations led to the fabrication and study of nanowires with widths in the 100's of nm range, with pinning sites composed of a half-circle notch defect with a radius of ~40% of the wire width. For example, the simulation results shown in Fig. 2 suggest that, for a 300 nm wide wire with a 120 nm defect, DW oscillations should be detectable at ~300 MHz below the NV ground state transition in the absence of an applied field, and that the two should come into resonance at a field below 10 mT. Simulations of the nanowire initialized with no DW present show that a DW nucleates between 11 and 12 mT applied field. This geometry thus allows for both DW detection and control measurements at fields below this threshold.

We now describe the measurements, focusing on two nanowire devices. Device 1 is a 300 nm wide nanowire with a 120 nm wide defect (a notch); device 2 is a 350 nm wide nanowire with a 140 nm wide defect. We use a pick-and-place protocol reported earlier[4] and in Methods to position a nanodiamond directly above the respective defect in each device (Fig. 3). We begin with a description of measurements on device 1.

---

[1]Department of Physics, The Pennsylvania State University, University Park 16802 PA, USA. [2]Department of Materials Science & Engineering, The Pennsylvania State University, University Park 16802 PA, USA. [3]Materials Research Institute, The Pennsylvania State University, University Park 16802 PA, USA. ✉email: nsamarth@psu.edu

Using the nanodiamond located at the defect in device 1, we begin measuring the DW nucleation field by monitoring the frequency of the NV ground state transition over increasing applied field with a continuous wave optically detected resonance (CW-ODMR) measurement (Fig. 4a). Because the Zeeman splitting is ~28 GHz/T $\vec{B} \cdot \hat{n}$, where $\vec{B}$ is the applied field and $\hat{n}$ is the NV axis unit vector, we can detect the nucleation and the accompanying increase in stray field at the pinning site via the detection of a discontinuity in the ground state transition. This is seen in Fig. 4a at 13 mT, slightly off from the predicted 11 mT from our simulations. Next, we search for DW oscillations using a pulsed ODMR measurement (Fig. 4b). In this measurement, we use the 532 nm laser to polarize the NV into the $m_s = 0$ state. We then apply microwaves for 5 µs with the laser off, and turn the laser back on to readout the state during the first 500 ns it is on (signal measurement). A reference measurement is then taken 15 µs later, after the NV spin is re-polarized, with the detected response as the contrast between the signal and reference measurements. By pulsing the laser off during the spin-relaxation period, we suppress any signals from the excited state spin transitions that could obscure a DW oscillation signal between 1–2 GHz; we also avoid repolarizing the NV spins during the relaxation period, improving measurement sensitivity. As a control measurement, we first sweep across a 400 MHz to 3.5 GHz range without
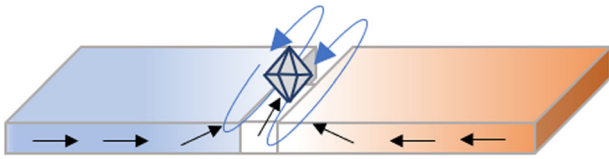
nucleating a DW (blue trace in Fig. 4c); this yields the expected result, with a single peak at the 2.87 GHz NV transition frequency and the accompanying lower frequency harmonics. In contrast, the experimental measurement with a DW nucleated (red trace in Fig. 4c), yields a broader range of dynamics than expected in simulations (Fig. 4d). Rather than a single broad peak centered at 2.4 GHz as predicted by simulations, we find two broad peaks at ~1.8 and 2.3 GHz, with an additional, sharper peak at 1.9 GHz. Earlier studies have suggested that DW dynamics in nanowires are extremely sensitive to edge roughness[12]. This leads us to hypothesize that the difference between experimental and simulated results is likely due to the deviation of the shape of the fabricated wires from the ideal design used in our simulations. Additionally, we hypothesize that the presence of multiple DW peaks could be the result of the ~1 mT microwave field amplitude used in our measurements. We note that previous experimental studies of single DW oscillation peaks do not report the excitation field strength[12,20]; thus, it is possible that the high driving power induces additional dynamics in wires with edge roughness. We also note that microwave-induced heating effects cannot explain the features that we attribute to DW oscillations since such heating effects would also be present in the control measurements in the absence of a pinned DW.

We might expect to obtain more insights into the DW oscillations by carrying out pulsed ODMR measurements as a function of increasing external magnetic field. This would also provide a route toward achieving resonant coupling. However, we find that the signal from the pulsed ODMR measurement in device 1 fades rapidly with increasing magnetic field, preventing us from exploring how the dynamics evolve with the field or realizing resonant coupling (data not shown). As we show later, device 2 behaves differently. Motivated by a prior report of vortex-mediated microwave power enhancement[11], we also performed Rabi oscillation measurements at the NV ground state transition frequency with and without a proximal DW. These measurements

Fig. 1 Schematic of the measurement concept. A nanodiamond containing NV centers is placed over a geometrically determined DW pinning site in a ferromagnetic nanowire.
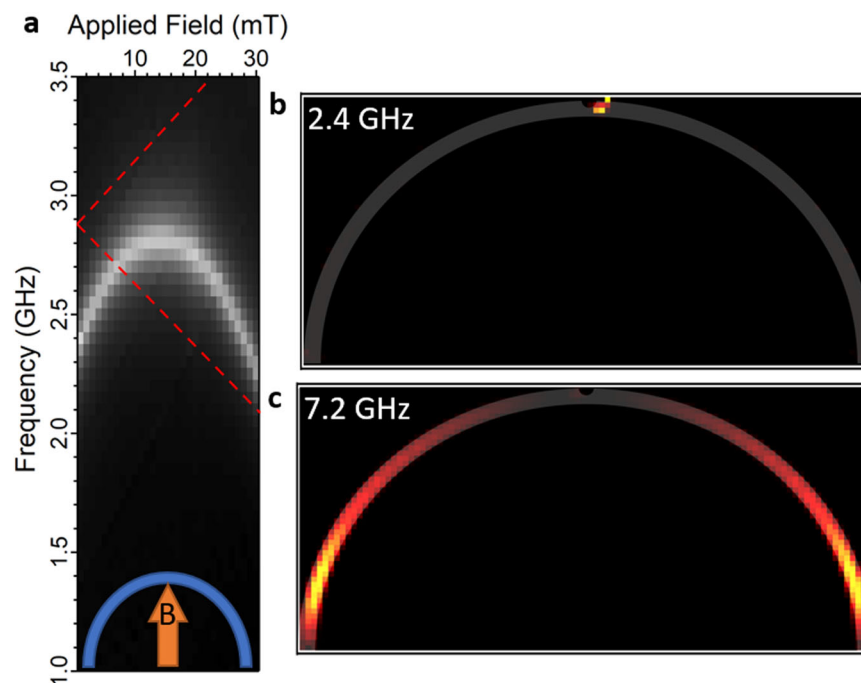

Fig. 2 Micromagnetics simulations of an oscillating DW pinned at a notch in a semicircular Py nanowire. a Simulated FFT amplitude showing the frequency of DW oscillations over applied fields in a 300 nm wide nanowire shaped into a semicircle (radius 2.5 µm) with a centrally positioned 120 nm radius half-circle defect. The dashed red lines show the calculated frequency of the NV ground state transition for a field perfectly aligned along the NV axis. The schematic at the bottom of the panel depicts the nanowire and magnetic field configuration. **b** Spatially resolved image of the FFT amplitude of the mode in **a** at 1 mT. **c** Spatially resolved image of the FFT amplitude of a higher frequency mode at 1 mT, showing that more uniform dynamics occur at much higher frequencies than DW dynamics.
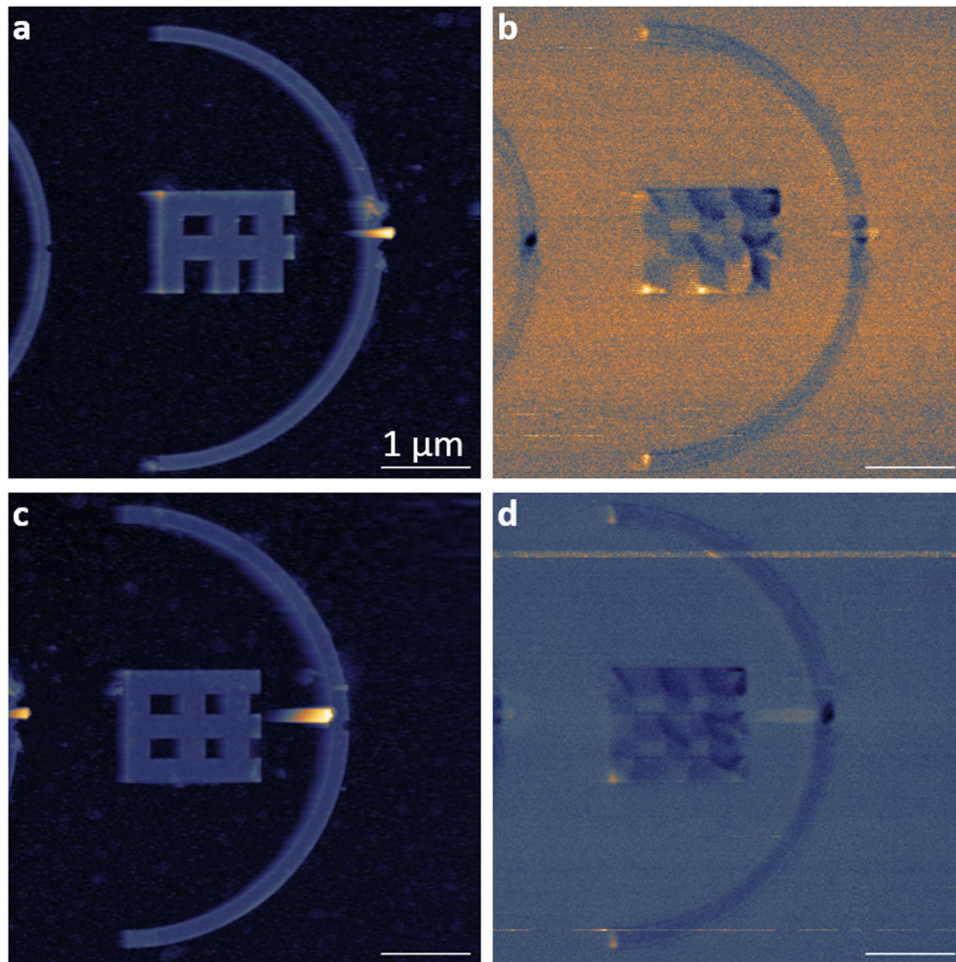
Fig. 3 AFM and MFM characterization of measured nanowire-notch-nanodiamond configurations. a Atomic force microscopy (AFM) image of nanodiamond placed at the pinning site (bright spot) in device 1, a 300 nm wide wire with a 120 nm radius half-circle defect. **b** MFM image of the same site, showing the presence of a DW (dark spot) near the nanodiamond and pinning site. The DW is partly obscured by the nanodiamond, which leaves a small bright streak on the image. **c** AFM image of nanodiamond placed at the pinning site in device 2, a 350 nm wide wire with a 140 nm radius half-circle defect. **d** MFM image of the same site, showing the presence of a DW in the wire.

failed to demonstrate DW-mediated power enhancement (Figs. S1, S2 in Supplementary Materials), and we do not see any signs of DW-mediated power broadening in our CW-ODMR signals (Fig. 4a). Additionally, we note that our simulations do not show the nucleation of vortex walls; even if we force a vortex wall configuration as the nucleated state, the resulting DW dynamics are around a few hundred MHz rather than GHz frequency range as observed in our experiments (Fig. S3 in Supplementary Materials).

We now discuss pulsed ODMR measurements of DW oscillations in device 2 (350 nm wide wire with a 140 nm defect, Fig. 3c). The results are shown in Figs. 5a and 6a. This wire does not appear ideal for resonant coupling in simulations (the frequency of the simulated DW oscillations does not overlap with the NV transitions in Fig. 6b). However, this is the largest in the series of nanowires we fabricated; thus, we expected it to produce the largest stray fields, making it a useful system to confirm our previous results. The control measurement without a DW (blue trace in Fig. 5a) shows the expected results, namely a peak at 2.87 GHz and accompanying harmonics, as in device 1. In the experimental measurement with a DW present (red trace in Fig. 5a), we see the strongest signal at ~2 GHz, like device 1, but again in some 20% disagreement with the simulations which predict a signal at 2.5 GHz. This result is surprising if we attribute the discrepancy between the experiment and simulations to nanofabrication-

related deviations from ideality (e.g., edge roughness): superficially, device 2 appears to have fewer fabrication errors compared to device 1 (Fig. 3a, c). We also detect additional peaks between 1.3–1.6 GHz and at 3.2 GHz. While the sharp peak at 1.4 GHz can be attributed to microwave harmonics and is seen in the control measurement, the other lower frequency peaks (at ~1.3 and 1.6 GHz) do not appear to be harmonics due to their wide frequency distribution and high contrast. At this stage, we do not have a rigorous explanation for the origin of these additional features. Since edge roughness is not an obvious explanation, a reasonable hypothesis is that nanodiamond creates inhomogeneous local mechanical strain in the nanowire. This could result in complex changes in magnetic anisotropy whose effects on the DW oscillations would not be captured by our idealized micromagnetic simulations.

Next, we discuss the magnetic field evolution of the pulsed ODMR data from device 2. Figure 6a shows that, in contrast to device 1, the DW oscillation signal at 2 GHz in device 2 survives in applied magnetic fields up to ~15 mT with an interesting evolution. With increasing field, this feature splits into two distinct features: one that increases in frequency but fades rapidly, and one that remains constant at 1.9 GHz. Neither of these match our simulated DW frequency dispersion and we do not have an explanation for the observed behavior. However, the persistent signal at 1.9 GHz can be exploited to detect the DW nucleation
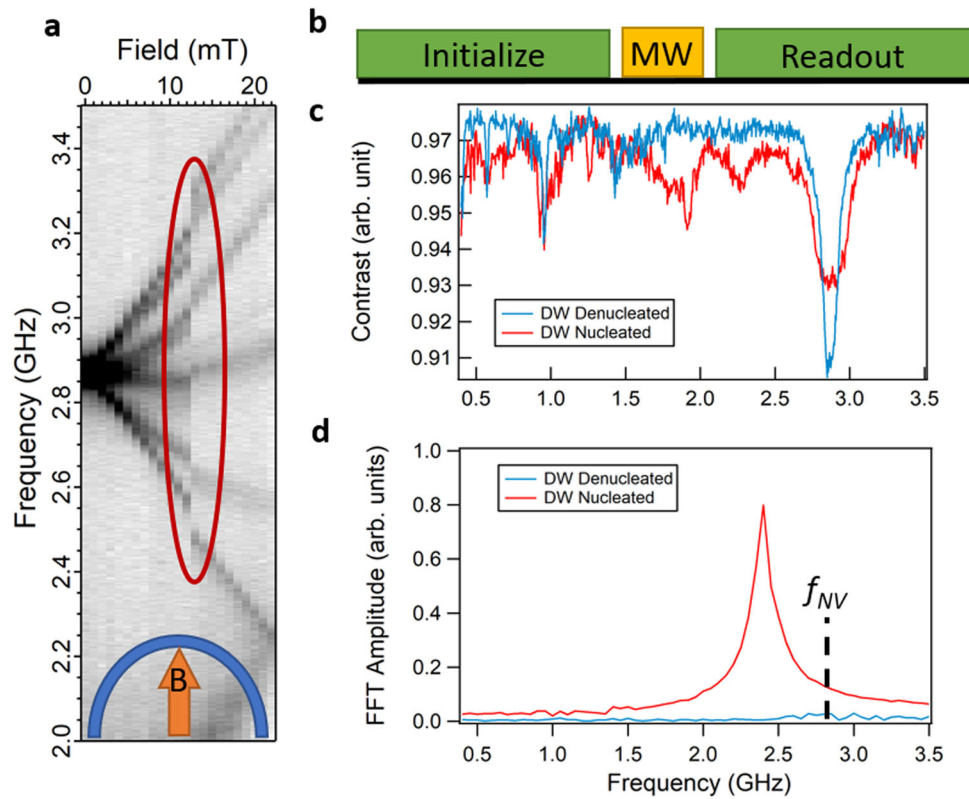
Fig. 4 NV center measurements of a pinned DW in device 1 using CW-ODMR and pulsed ODMR. a Optical contrast in a CW-ODMR measurement performed on a nanodiamond positioned over the pinning site of a 300 nm wide nanowire with a 120 nm defect (device 1). The circled discontinuity marks where the DW nucleated. **b** Schematic of the pulsed ODMR measurement used to detect DW dynamics; green blocks denote the 532 nm laser. MW refers to the microwave excitation pulse. **c** Pulsed ODMR measurements of the nanodiamond from **a** were performed both with a nucleated DW and without in a minimal applied field (0.7 mT). **d** Normalized line cut of FFT amplitudes from the simulation results in Fig. 2a at 1 mT, along with the normalized FFT amplitudes of a simulation in the same wire without a DW nucleated.

field using a dynamical measurement rather than a static one as discussed earlier (e.g., Fig. 4). We demonstrate this in Fig. 6c where we monitor the pulsed ODMR as a DW is nucleated. The nucleation field is indicated by the sudden appearance of a pulsed ODMR signal ~1.9 GHz when the applied magnetic field is 11.25 mT, matching our simulations that show nucleation occurs between 11 and 12 mT. Thus, while our dynamic simulations fail to accurately predict DW oscillation frequency in device 2, our quasi-static simulations accurately predict the nucleation field of the DW. Despite the disagreement between the experiment and simulations, it is clear from our control measurements that the features we observed in pulsed ODMR measurements must arise from the presence of the pinned DW.

DISCUSSION

An interesting question arises from our observations: what is the physical mechanism responsible for the spin-relaxation of NV centers in the presence of off-resonant DW dynamics? To address this question, we perform an additional series of power-dependent micromagnetic simulations and power-dependent measurements of the DW signal on the 300 nm diameter wire. In these simulations, we drive the DW with a resonant 2.4 GHz microwave excitation and extract the time-dependent AC stray field produced at a location 50 nm above the pinning site, where the average NV center would be located in our experiments. By analyzing the Fourier components of the produced field, we can determine the strength of the DW-generated field at higher frequencies, including the NV ground state transition frequencies, to see if they are strong enough to induce spin-relaxation. We can then compare these results qualitatively to corresponding power-

dependent experimental measurements. For these NV measurements of the DW signal, we perform pulsed ODMR measurements at different applied microwave powers and approximate the strength of the DW-generated field at the NV transition frequency using the contrast it produces at 1.9 GHz. The microwave driving power at the DW oscillation frequency in these measurements is estimated from Rabi oscillation measurements at the NV at the ground state transition frequencies.

Fourier components extracted up to 4 GHz from the 2.4 GHz DW oscillation generated stray field in our simulations exceeded magnitudes of 0.1 mT at driving powers achieved in our experiments, making the AC noise generated large enough to explain our measured contrast. Furthermore, comparing these results to our power-dependent measurements of DW oscillation-induced contrast in Fig. 7, we see that, while the results do not match quantitively, they exhibit a qualitatively similar pattern of behavior. Thus, the most likely explanation for off-resonant detection of DW oscillations with NV centers appears to be the generation of broadband AC noise at higher frequencies, like the previously reported results for vortex gyrations[7].

Additionally, extracting the Fourier component of the DW-generated microwave field in the power-dependent simulations at the driving field frequency shows a strong enhancement of the applied field above the pinning site (see Fig. S4 in Supplementary Materials). Driving fields of 0.1 mT magnitude result in a simulated stray microwave field amplitude exceeding 3 mT at the DW oscillation frequency, suggesting that bringing a DW and NV center into resonance can drastically reduce the π pulse time. These simulations provide a strong motivation for realizing resonant coupling using the platform and methodology we have described.
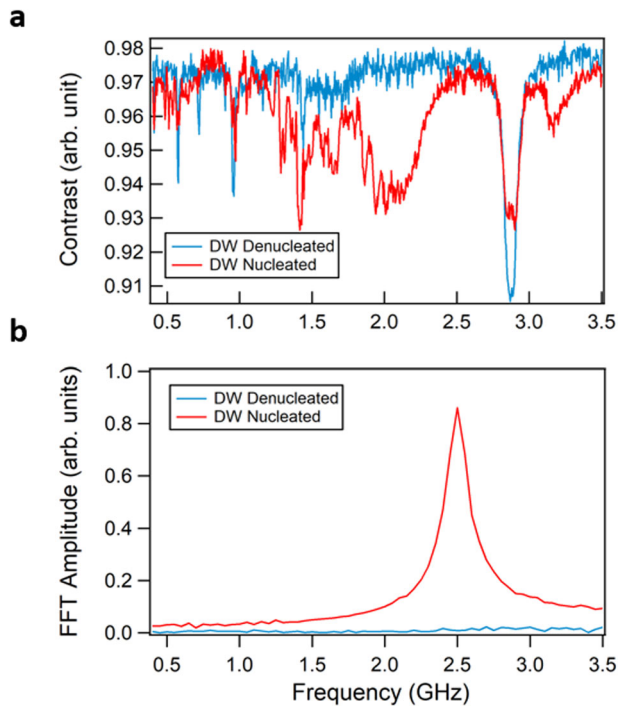
a

b

Fig. 5 Pulsed ODMR measurements and simulations of oscillations of a pinned DW in nanowire device 2. a Pulsed ODMR measurement on the nanodiamond in Fig. 3c, located on top of a 350 nm wide wire with a 140 nm radius semicircular defect. **b** Normalized FFT amplitudes from simulations of dynamics in a 350 nm wide bowed wire with a 140 nm radius semicircular defect with and without a DW.

In summary, we have demonstrated NV center-based detection of localized GHz-scale DW dynamics in a ferromagnet by deterministically placing a nanodiamond on top of a DW pinning site in Py nanowires. This detection, via enhanced spin-relaxation from the broadband stray field noise generated by the oscillating DW, further expands the menagerie of magnetic dynamics that can be measured using NV centers. Additionally, the prospect of resonant NV-DW coupling opens up potential avenues for qubit control; in the microwave-driven case, our simulations suggest that the presence of a proximal, resonant DW could increase the driving field at an NV center by over a factor of 30, drastically reducing the π pulse time. Finally, this work opens up the possibility of driving NV centers using current-driven DW oscillations in these nanowires, exploiting DWs as nanoscale microwave generators.

METHODS

Domain wall oscillation measurement

We use standard electron beam lithography, electron beam thin film deposition, and a liftoff process to prepare 10 nm thick Py semicircular nanowires with a notch-shaped defect in the center. 100 nm diameter nanodiamonds (Adámas Nanotechnologies, 3 ppm NV) are placed using an AFM pick-and-place technique outlined elsewhere[4], yielding results like those shown in Fig. 3a, c. MFM measurements, carried out in a Bruker ICON AFM with a low moment CoCr coated tip (Bruker, MESP-LM-V2), confirm nanodiamond proximity to a DW (Fig. 3b, d). DWs in the nanowires are created and destroyed using the shape anisotropy of the curved wires; they are nucleated by applying a magnetic field perpendicular to the wire at the defect site, and denucleated by applying a magnetic field tangential to the wire at the defect site. The in-plane nucleation field is applied using an N52 permanent magnet

mounted on a highly repeatable stepper motor stage (Newport, ILS200PP Stepper Motor), and the denucleation field is applied using an N52 magnet positioned near the sample by hand. The nucleation magnetic field is calibrated in the plane of the sample using the NV centers in a single crystal CVD diamond film with known orientation; due to stage limits, the smallest field we can apply is 0.7 mT.

For optical polarization and readout of the NV center fluorescence, we use excitation via a 532 nm wavelength CW laser (Oxxius, LCX-532L-200-CSB-PP) and detection with an avalanche photodiode (ID Quantique, ID100). The laser is pulsed using an acousto-optical modulator (Gooch and Housego, 15210) set up in a double pass configuration, scanned across the sample via a fast scanning mirror (Optics in Motion, FSM-101), and focused on the sample using a 100 × 0.9 numerical aperture (NA) objective lens (Nikon, 100 × Plan Fluor 0.9 NA objective). During the measurements, we apply a microwave magnetic field, which drives both NV spin transitions and magnetization dynamics, via a microwave signal generator (Stanford Research, SG396), +43 dBm amplifier (Mini-Circuits, ZHL-16W-43-S+), and a 25 μm diameter gold wire placed across the sample.

Micromagnetic simulations

We perform micromagnetic simulations to design our nanowires and to eventually compare them to our experimental results. These simulations are performed with the Mumax3 software package, which uses the Landau-Lifshitz-Gilbert equation:

$$\frac{\partial \vec{M}}{\partial t} = \gamma_{LL} \frac{1}{1+\alpha^2}(\vec{m} \times \vec{B}_{eff} + \alpha(\vec{m} \times (\vec{m} \times \vec{B}_{eff}))) \quad (1)$$

to calculate the evolution of the magnetization $\vec{M}$ of finite ferromagnetic cells. In Eq. (1), α is the Gilbert damping of the material, γ_{LL} is the gyromagnetic ratio of the material, and B_{eff} is the effective magnetic field at that cell, which includes contributions from external, demagnetization, exchange, and anisotropy fields[21].

The simulations use 5 nm × 5 nm × 10 nm cells with a saturation magnetization M_s of 8×10^5 A/m, an exchange constant A_{ex} of 1.3×10^{-11} J/m, and a Gilbert damping parameter α of 0.0063, which are standard for Py.

After defining the wire geometry, initial simulations of DW nucleation are performed by giving the system a constant (1, 0, 0) magnetization (pointing tangential to the wire direction at the defect site) with an applied magnetic field along the (0, 1, 0) direction. The system is then allowed to relax into a low-energy state. At low fields, the magnetization continues to lie along the wire direction, but past a certain field, a transverse DW nucleates in the wire due to shape anisotropy. The magnetization of the nucleated state is used as the initial state for the DW dynamics simulations. In these simulations, the nucleated magnetization from the previous simulations is loaded, and then allowed to relax in an applied field, like before.

To excite the system, we then apply a Gaussian pulse with a 20 ps full-width half maximum (FWHM) and a 0.5 mT amplitude. The system is allowed to freely evolve in time for 20 ns and the average magnetization is sampled every 5 ps. Finally, we use a discrete fast Fourier transform (FFT) to analyze the data in the frequency domain, providing a resolution of 50 MHz and window from 0 to 100 GHz, well beyond the range of interest in this work.

For spatially resolved simulations, a shorter 1 ps FWHM pulse is used, and the magnetization is sampled in discrete 50 × 50 nm blocks composed of 100 cells. The average magnetization of each block is analyzed using an FFT as before and the image is composed of each block's FFT amplitude at the desired frequency.

To determine the time-dependent AC stray field produced by a DW, we drive the system at a constant microwave frequency for 20 ns and sample the magnetization of every cell within 500 nm of the pinning site every 5 ps. Then, treating every cell as an
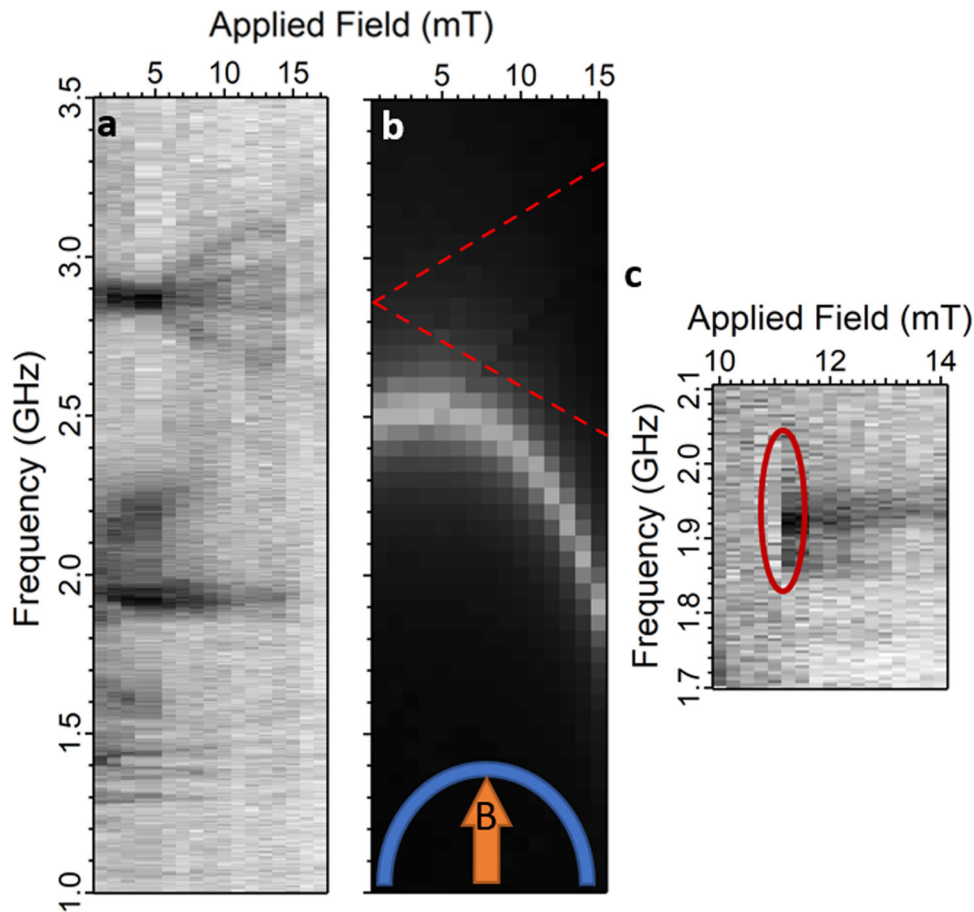
Fig. 6 Pulsed ODMR detection of magnetic field-dependent oscillations and nucleation of a pinned DW in nanowire device 2. a Pulsed ODMR measurement of the pinned DW in device 2 performed as a function of applied field. **b** Simulated FFT amplitudes of the DW dynamics of the nanowire measured in **a**; the dashed red line represents the NV ground state transition frequency for an applied field oriented perfectly along the NV axis. **c** Pulsed ODMR detection of DW nucleation in nanowire device 2 using the 1.9 GHz peak; the nucleation field is circled in red.
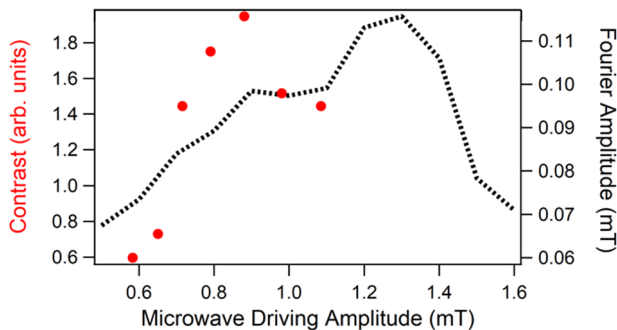
Fig. 7 Measurement and simulation of the power dependence of DW oscillations. NV center DW oscillation peak contrast (red dots) in the 300 nm wide wire and the corresponding simulated stray field Fourier component magnitude at 3.3 GHz (dashed line) versus microwave driving field amplitude. 3.3 GHz was selected for this plot because it is 0.9 GHz above the DW oscillation frequency in our simulations, matching the frequency gap between our measured oscillation peak and the NV transition frequencies. The simulated DW stray field used to perform this analysis was measured at 50 nm above the center of the wire, where the pinning site was located.

individual dipole, we solve for the magnetic field at the desired location by summing the individual dipole fields at each time point. An FFT can then be used to determine the microwave field's frequency distribution.

DATA AVAILABILITY
All raw data are available upon request.

REFERENCES

1. Wolfe, C. S. et al. Off-resonant manipulation of spins in diamond via precessing magnetization of a proximal ferromagnet. *Phys. Rev. B* **89**, 180406 (2014).
2. Page, M. R. et al. Optically detected ferromagnetic resonance in diverse ferromagnets via nitrogen vacancy centers in diamond. *J. Appl. Phys.* **126**, https://arxiv.org/abs/1607.07485 (2019).
3. Du, C. et al. Control and local measurement of the spin chemical potential in a magnetic insulator. *Science* **357**, 195–198 (2017).
4. Rable, J., Piazza, B., Dwivedi, J. & Samarth, N. Local ferromagnetic resonance measurements of mesoscopically patterned ferromagnets using deterministically placed nanodiamonds. *Phys. Rev. Appl.* **18**, 064004 (2022).
5. Zhou, T. X. et al. A magnon scattering platform. *PNAS* **118**, e2019473118 (2021).
6. Koerner, C. et al. Frequency multiplication by collective nanoscale spin-wave dynamics. *Science* **375**, 1165–1169 (2022).
7. Trimble, J. et al. Relaxation of a single defect spin by the low-frequency gyrotropic mode of a magnetic vortex. *J. Appl. Phys.* **130**, 083903 (2021).
8. Andrich, P. et al. Long-range spin wave mediated control of defect qubits in nanodiamonds. *npj Quantum Inf.* **3**, 28 (2017).
9. Wang, X. et al. Electrical control of coherent spin rotation of a single-spin qubit. *npj Quantum Inf.* **6**, 78 (2020).
10. Yan, G. Q. et al. Electric-field-induced coherent control of nitrogen-vacancy centers. *Phys. Rev. Appl.* **18**, 064031 (2022).

11. Wolf, M. S., Badea, R. & Berezovsky, J. Fast nanoscale addressability of nitrogen-vacancy spins via coupling to a dynamic ferromagnetic vortex. *Nat. Commun.* **7**, 11584 (2016).

12. Galkiewicz, A. T., O'Brien, L., Keatley, P. S., Cowburn, R. P. & Crowell, P. A. Resonance in magnetostatically coupled transverse domain walls. *Phys. Rev. B* **90**, 024420 (2014).

13. Demiray, A. S., Naganuma, H., Oogane, M. & Ando, Y. Optimization of domain wall oscillations in magnetic nanowires. *IEEE Magn. Lett.* **6**, 1–4 (2015).

14. Sbiaa, R., Bahri, M. A. & Piramanayagam, S. N. Domain wall oscillation in magnetic nanowire with a geometrically confined region. *J. Magn. Magn. Mater.* **456**, 324–328 (2018).

15. Saitoh, E., Miyajima, H., Yamaoka, T. & Tatara, G. Current-induced resonance and mass determination of a single magnetic domain wall. *Nature* **432**, 203–206 (2004).

16. Kumar, D., Sengupta, P., Sbiaa, R. & Piramanayagam, S. N. Spin transfer torque induced domain wall oscillations in ferromagnetic nanowire with a nanoscale Dzyaloshinskii-Moriya interaction region. *J. Magn. Magn. Mater.* **507**, 166807 (2020).

17. Tetienne, J.-P. et al. The nature of domain walls in ultrathin ferromagnets revealed by scanning nanomagnetometry. *Nat. Commun.* **6**, 6733 (2015).

18. Finco, A. et al. Imaging non-collinear antiferromagnetic textures via single spin relaxometry. *Nat. Commun.* **12**, 767 (2021).

19. Jenkins, A. et al. Single-spin sensing of domain-wall structure and dynamics in a thin-film skyrmion host. *Phys. Rev. Mater.* **3**, 083801 (2019).

20. Volodin, A., Van Haesendonck, C., Skorokhodov, E. V., Gorev, R. V. & Mironov, V. L. Ferromagnetic resonance force microscopy of individual domain wall. *Appl. Phys. Lett.* **113**, 122407 (2018).

21. Vansteenkiste, A. et al. The design and verification of MuMax3. *AIP Adv.* **4**, https://arxiv.org/abs/1406.7635 (2014).

AUTHOR CONTRIBUTIONS

J.R. and N.S. conceived the idea for this project. J.R. and J.D. carried out the experiments and analyzed the data with input from N.S. who also supervised the project. All authors discussed the results. J.R. and N.S. wrote the manuscript with contributions from J.D.

COMPETING INTERESTS

The authors declare no competing interests.

ADDITIONAL INFORMATION

Supplementary information The online version contains supplementary material available at https://doi.org/10.1038/s44306-023-00002-3.

Correspondence and requests for materials should be addressed to Nitin Samarth.

Reprints and permission information is available at http://www.nature.com/reprints

Publisher's note Springer Nature remains neutral with regard to jurisdictional claims in published maps and institutional affiliations.